Quaternary Science Reviews 320 (2023) 108355

Contents lists available at ScienceDirect

Quaternary Science Reviews

journal homepage: www.elsevier.com/locate/quascirev

A mid-Holocene stalagmite multiproxy record from southern Siberia (Krasnoyarsk, Russia) linked to the Siberian High patterns

A. Columbu [a,b,*], L.V. Zhornyak [a], G. Zanchetta [a,b,c], R.N. Drysdale [e], J.C. Hellstrom [f], I. Isola [b], E. Regattieri [g], A.E. Fallick [h]

[a] Dipartimento di Scienze della Terra, University of Pisa, Via S. Maria 53, 56126 Pisa, Italy
[b] CIRSEC-Centre for Climatic Change Impact, University of Pisa, Dipartimento di Scienze Agrarie, Alimentari e Agro-ambientali, Via del Borghetto 80, 56124, Pisa, Italy
[c] Instituto Nazionale di Geofisica e Vulcanologia, Sezione di Pisa, Via della Faggiola 32, 56126, Pisa, Italy
[e] Department of Resource Management and Geography, University of Melbourne, Victoria, 3010, Australia
[f] School of Earth Sciences, University of Melbourne, Victoria, 3010, Australia
[g] Istituto di Geoscienze e Georisorse, Via Cesare Battisti 53, 56125, Pisa, Italy
[h] Scottish Universities Environmental Research Centre, East Kilbride G75 0QF, United Kingdom

ARTICLE INFO

Handling Editor: Mira Matthews

Keywords:
Stable isotopes
Fluorescence
Speleothems
Siberian high
Holocene
Permafrost
Paleoclimate
4.2 event

ABSTRACT

A multiproxy record from a stalagmite collected from Torgashinskaya Cave (Southern Siberia, Russia) and growing between ca. 6 and 3.8 ka shows evidence for regional climatic changes occurring at ca. 5 ka. Interpretation of stable isotope ratios ($\delta^{18}O$ and $\delta^{13}C$) and fluorescence data (intensity and wavelength of the emitted fluorescence) suggests that the interval between ca. 5 and 4.2 ka was generally warmer and drier than the interval between ca. 6 and 5 ka. The observed bipartitioning of the climate, attributable to the so-called 'middle-late Holocene transition', has a striking similarity to changes in K^+ and Na^+ concentration of Greenland ice cores (taken as indicators of the strength of the Siberian High and Icelandic Low, respectively), in the abundance of hematite-stained grains in subpolar North Atlantic sediments and, to lesser extent, in the summer Asian monsoon intensity deduced by $\delta^{18}O$ from Chinese speleothems. In particular, the $\delta^{18}O$ record at Torgashinskaya Cave can be interpreted as mostly driven by temperature changes. Besides several episodes of drift towards higher temperatures, it also strongly suggests the presence of short cooling events centered at $4.1^{+0.08}/_{-0.07}$, $4.85^{+0.05}/_{-0.06}$, $5.1^{+0.09}/_{-0.09}$, $5.3^{+0.08}/_{-0.07}$ and $5.8^{+0.12}/_{-0.13}$ ka. Notably, the last three such events are in very good correspondence with spikes in the K^+ and Na^+ concentration of Greenland ice cores. Instead, the cooling around 4.1 ka could be the local response to the 4.2 event, a cold/dry episode identified in several records in the Northern Hemisphere. This suggests that $\delta^{18}O$ of speleothem calcite from this area could be a useful proxy for defining the evolution of the Siberian High and its effect on the wider regional climate.

1. Introduction

Southern Siberia represents a crucial region for palaeoclimate studies. The area is situated deep inside the Asian continent, where winter conditions are particularly severe because of the dominance of the Siberian High (SH). This strong semi-permanent anticyclonic circulation system is centered over Mongolia and Southern Siberia, and defined as the regional mean sea level pressure (SLP) averaged over the 70°E–120°E and 40°N-60°N area (Cohen et al., 2001; Gong and Ho, 2002). Its impact on circulation, temperature and snow cover extends well beyond its source area, spreading north to the Arctic, south to south Asia and the tropical Pacific (where it influences the East Asian Winter Monsoon/Australian-Indonesian Summer Monsoon), and westwards into the Mediterranean region (Cohen et al., 2001; Gong and Ho, 2002; Wu and Wang, 2002; Panagiotopoulos et al., 2005; Riaz et al., 2018; Labban et al., 2021). Analyses of temperature patterns indicate that the intensity of the SH is correlated with the state of the Arctic Oscillation, with enhanced cyclogenesis over the eastern flank of the Iceland Low (IL) associated with milder SH conditions (Tubi and Dayan, 2013).

Comprehending the patterns and evolution of the SH through time is key given its significance in the climatology of the Eurasian landmass, where it interplays with the westerlies and the monsoonal climatic systems (Cheng et al., 2016). Yet, most of the previous research has been conducted in regions on or beyond the margins of highest SH pressure.

* Corresponding author. Dipartimento di Scienze della Terra, University of Pisa, Via S. Maria 53, 56126, Pisa, Italy.
E-mail address: andrea.columbu@unipi.it (A. Columbu).

https://doi.org/10.1016/j.quascirev.2023.108355
Received 4 September 2023; Received in revised form 10 October 2023; Accepted 10 October 2023
Available online 14 October 2023
0277-3791/© 2023 The Authors. Published by Elsevier Ltd. This is an open access article under the CC BY-NC-ND license (http://creativecommons.org/licenses/by-nc-nd/4.0/).

As an example, it has been proposed that periods of significant westward extension of the SH were responsible for episodes of cooling during the Holocene in the Aegean sector of the Mediterranean region (Rohling et al., 2002; Marino et al., 2009). These coolings stimulated local cyclogenesis, affecting precipitation amount and regime in the Levant and in the Middle East (Rohling et al., 2019; Regattieri et al., 2023). Some hydrological effects of a stronger SH, related to blocking configuration and changes in storm track trajectories, have been proposed also to extend to Central Europe (Perşoiu et al., 2019) and to the Balkan Peninsula (Regattieri et al., 2019). Potassium ion (K^+) concentration variability in Greenland ice (GISP) has been related to dust transport from Asia, and interpreted as a proxy for SH intensity, showing significant changes in its strength during the Holocene (Mayewski et al., 1997; Meeker and Mayewsky, 2002). Furthermore, titanium concentrations and mineral magnetic properties in the Lake Huguang maar recorded changes in the strength of Asian Winter Monsoon northerly winds over the last 16 kyr, that are in turn related to the strength of the SH (Yancheva et al., 2007), and also exert an important effect in controlling the strength of the Australian-Indonesian Summer Monsoon (Griffiths et al., 2009). These records can therefore be used as a benchmark for comparison with Holocene climate proxy records from the core region of the SH.

On the other hand, there is a paucity of records from the core region of the SH that currently experiences the coldest winter conditions, and the chronological constraints of the existing records is inadequate for the study of rapid climate shifts (Mikhailova et al., 2021 and references therein). This is even more compelling nowadays, considering the impact of current global warming on permafrost or peri-permafrost regions (Turetsky et al., 2020). High resolution palaeoclimate proxy time series from Southern Siberia offer therefore the chance to investigate the local expression of SH variability, as well as to uncover climate teleconnections with regions situated beyond the high-pressure core.

Speleothems (cave calcite deposits) are powerful tools for terrestrial palaeoclimatic and palaeoenvironmental reconstructions (Fairchild et al., 2006; Fairchild and Baker, 2012), with carbon ($\delta^{13}C$) and oxygen ($\delta^{18}O$) stable isotopes ratios often related to several parameters including soil bioproductivity, atmospheric temperatures, rainfall amount, moisture source and trajectories (Ait Brahim et al., 2019; Moseley et al., 2020; Della Libera et al., 2022; Dong et al., 2022; Fohlmeister et al., 2023). However, in regions with mean annual temperatures below 0 °C, speleothem growth can be very slow or non-existent (e.g. Berstad et al., 2002; Vaks et al., 2013; Lechleitner et al., 2020) considering: i) the necessity of liquid water percolating through the bedrock; and ii) the need for a developed soil as CO_2 source to the infiltrating water. Notwithstanding this, if water infiltration is somehow active, speleothem deposition can be locally triggered by processes not requiring biogenic CO_2 input from soils, such as by pyrite oxidation enhancing rock dissolution in the epikarst and then favouring calcite precipitation deeper in the cave (e.g Spötl and Mangini, 2007; Regattieri et al., 2014; Bajo et al., 2017). In the peri-Arctic and Arctic Region, speleothem growth is reduced or absent during periods of continuous permafrost and/or scarce soil cover (Linge et al., 2001; Vaks et al., 2013); accordingly, caves are not as well decorated as those in more temperate settings (De Waele and Gutiérrez, 2022), and cave calcite can be rare. It follows that speleothem growth *per se* is considered as evidence for the absence of permafrost and for the occurrence of climatically favorable conditions (i.e. warmer and/or wetter) during for example interglacials and/or interstadials. For this reason, much of the work on speleothem from these latitudes has been focused in chronologically constraining the evolution of permafrost (Wilcox et al., 2019; Lechleitner et al., 2020), especially in Siberia (Vaks et al., 2013, 2020), rather than exploiting speleothem stable isotope ratios – among others - for producing climate-proxy time series. In this regard, speleothem proxy records are still scarce in Siberia and, to our knowledge, only one record is available (Li et al., 2021) covering the early Holocene. This is unfortunate as during the permafrost-free periods cave archives could offer important insights for elucidating climatic evolution of this latitudinal bridge between North Atlantic-dominated and monsoon-dominated regions.

With the aim of starting to fill these gaps, this work presents a decadal resolved, multiproxy record obtained from the TO1 stalagmite (Torgashinskaya Cave, Southern Siberia, Russia). U–Th radiometric dating reveals that the deposition occurred between ca. 6 and 4 thousand of years before 1950 CE (hereafter ka). This period is of particular interest because records outside the SH core area suggest a substantial reorganization of climate, during the so-called 'middle-late Holocene transition' (Debret et al., 2009; Wirtz et al., 2010; Fletcher et al., 2013; Magny et al., 2013; Zhang et al., 2019). By interpreting the significance of TO1 $\delta^{13}C$-$\delta^{18}O$ timeseries, along with its fluorescence properties, this paper aims to: 1) understand the climate and environmental meaning of $\delta^{13}C$-$\delta^{18}O$ in speleothems from this area, given the scarcity of information in this regard; and 2) provide the first speleothem-based middle-to-late Holocene paleoclimate reconstruction for this underexplored area. By doing so, we are able to explore the role of the SH variability on Southern Siberia climate during the middle to late Holocene transition.

2. Study area

Torgashinskaya Cave (55° 55′28.1″ N, 92° 57′00.4″ E, Fig. 1) is situated in the southern part of Siberia, close to the town of Krasnoyarsk. The area lies between the Central Siberian plateau (right bank of the Yenisei River), the West Siberian Plain (left bank of the Yenisei River) and the Sayan and Altai Mountains. The cave is located in the foothills of the Eastern Sayan Mountains within the karst zone lying between the Yenisei River and its tributary, the Bazaikha. Torgashinskaya Cave has a funnel-shaped entrance at about 500 m a.s.l., and extends over a total length of 2965 m. The cave is carved within Lower to Middle Cambrian light-grey massive limestone. Passages within the cave have been developed mainly along fractures of tectonic origin. At the entrance shaft, there is a permanent ice-snow plug. The temperature inside the cave ranges from +1.9 to +3°C, and humidity ranges between 97 and 99%. The recharge area of the cave is ca. 2.5 ha. The surface is covered by taiga with a grey mountain forest soil; nearby, sporadic permafrost occurs (Fig. 1).

The climate of the area is extremely continental and mainly controlled by Siberian air masses, by warm and wet winds of Atlantic origin, and by warm southwesterly winds that bring air from Central Asia. In winter, Southern Siberia is influenced by the semi-permanent SH, which begins to build up at the end of August, reaches its peak during winter, and remains strong until the end of April (Cohen et al., 2001; Gong and Ho, 2002; Wu and Wang, 2002; Panagiotopoulos et al., 2005). The average annual temperature (30 years from 1960 to 1990, http://meteoinfo.ru/KrasnoyarskClimat) measured in the town of Krasnoyarsk is about 1 °C, with a July average of +18.5 °C and a January average of −15.6 °C (Fig. 1). From early April to late October the temperature usually remains persistently above 0 °C. The mean annual precipitation is ca. 465 mm, with a minimum in February and a maximum in July (Fig. 1). The temperature range during the year can exceed 55 °C. Snow cover is usually present from the end of October until the beginning of April.

3. Materials and methods

TO1 is a 26 cm long stalagmite (Fig. 2) that was collected *in situ* in the deepest part of the cave, at a depth of about 170 m below the entrance level (Fig. 1). Thick clay layers on the floor and the presence of pools in the terminal chamber indicate the occurrence of occasional flooding. TO1 was sectioned parallel to the growth axis and analyzed for petrography, stable carbon and oxygen isotope ratios ($\delta^{13}C$ and $\delta^{18}O$), and UV fluorescence properties (intensity and the peak emission wavelength). A total of 141 samples for stable isotope analysis were extracted along the growth axis from a polished quarter of the stalagmite

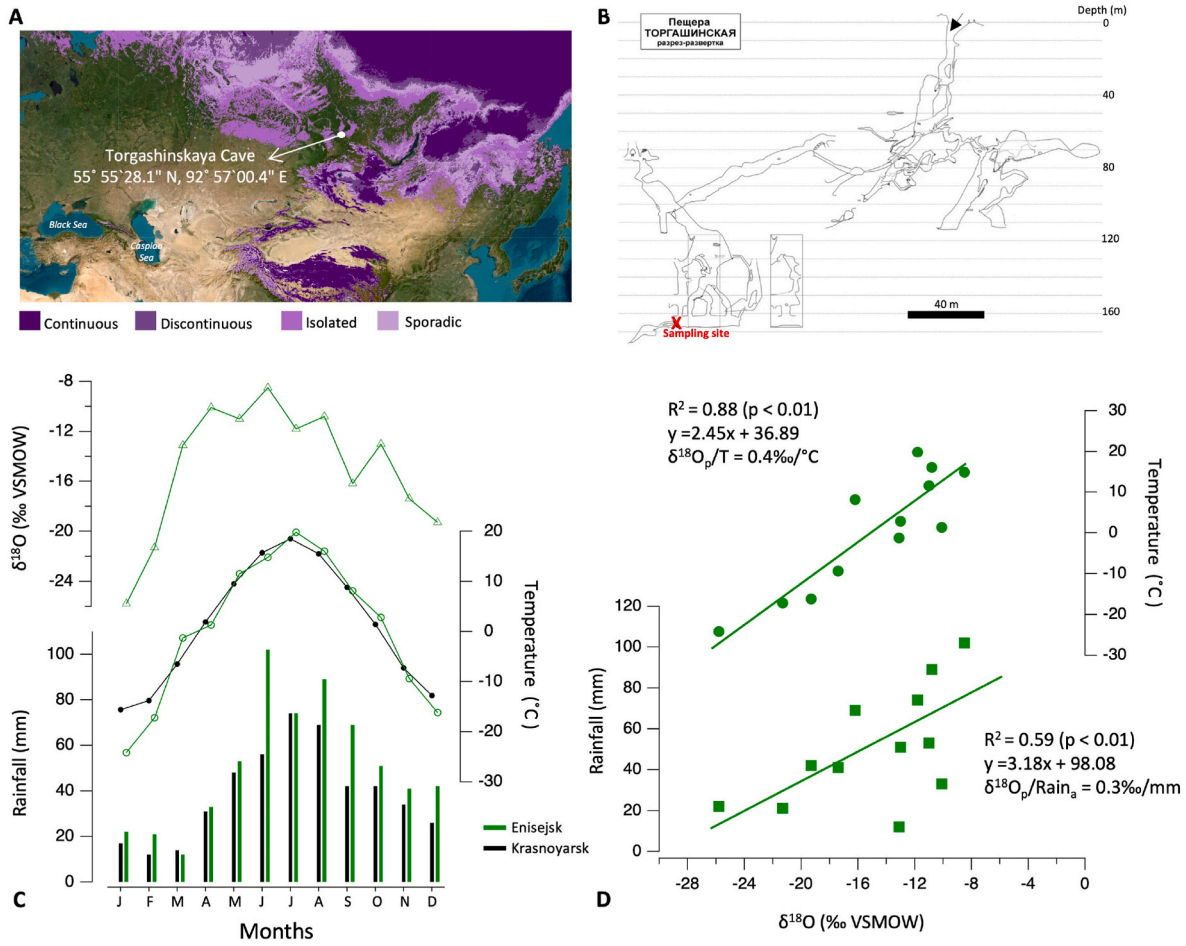

Fig. 1. Area of study. A) Location of Torgashinskaya Cave, with coordinates. The extension of permafrost is taken from www.globpermafrost.info. B) Section of the cave, with the sampling site at around 160 m below the surface. C) Monthly-mean meteorological data from Krasnoyarsk (black lines) and Enisejsk (green lines) stations. Rainfall $\delta^{18}O$ data are only available for the latter. D) Correlation between rainfall precipitation $\delta^{18}O$ ($\delta^{18}O_p$), temperatures (T) and rainfall amount ($Rain_a$) at Enisejsk. Data are from http://meteoinfo.ru/KrasnoyarskClimat and http://ishohis.iaea.org for Krasnoyarsk (30 years monthly average, 1960–1990) and Enisejsk (1 year monthly average, 1990) respectively.

using an hand-held microdrill with a 1 mm drill bit. The average interval between samples is 1.8 mm. To determine whether the calcite was affected by isotopic disequilibrium, samples were also taken along two individual growth layers for the "Hendy test" (Hendy, 1971).

The stable isotope composition of the carbonate powders was measured on CO_2 gas released by reaction with 105% H_3PO_4 at 70 °C using an AP2003 mass spectrometer at the Scottish Universities Environmental Research Centre (East Kilbride, UK). Isotopic results are reported in conventional δ-notation *per mil* (‰), with reference to the Vienna Pee Dee Belemnite (V-PDB) standard. Precision was monitored by incorporating internal laboratory marble standards (MAB 1) with each batch of analyses, and calibration was *via* NBS 19 carbonate; precision (±1σ) was better than 0.1‰ for both carbon and oxygen isotope ratios.

Fluorescence was measured directly on the polished slab of the stalagmite using a fibre-optic probe coupled to a Varian Cary Eclipse Fluorescence Spectrophotometer in the laboratory of the University of Newcastle, NSW, Australia. The fluorescence scan commenced at the top of the stalagmite and ran parallel to the stable isotope sampling traverse but at a ca. 3 mm offset. Due to the 4-mm spot size of the probe, the central point of the first and the last observations is 2 mm from the top and bottom of the slab, respectively. Consecutive fluorescence measurements were carried out by moving of the speleothem slab under the fibre-optic probe via a motorised stage at a ca. 2 mm step for the upper 10 cm and a 3 mm step for the lower 16 cm. For each sample point, ultraviolet excitation energy in the 300–400 nm wavelength (λ) range (supplied from a xenon flash lamp) illuminated the sample in 2 nm steps via the fibre-optic probe. The resulting emission intensity was detected at 1 nm steps between 380 and 480 nm. The excitation and emission slits were set at 5 nm and the lamp energy fixed at 700 PMT voltage. The data reduction method followed the procedure outlined in Drysdale et al. (2006).

Thin sections were obtained for the central part of TO1 and analyzed using a petrographic microscope. Crystal fabric description generally follows the terminology of Frisia et al. (2015).

The chronology of TO1 is based on ten U–Th dates (Fig. 2) derived from 20 to 30 mg of calcite extracted using a 1 mm drill bit. Samples were measured using a Nu-Instruments multi-collector inductively coupled plasma mass spectrometer (MC-ICP-MS) at the University of Melbourne (Australia). The methodology is described in detail by Hellstrom (2003). Briefly, prior to the analysis, sub-samples were dissolved with concentrated nitric acid and equilibrated with a $^{229}Th/^{233}U$ mixed-spike solution; subsequently, uranium and thorium were separated from the carbonate matrix using Eichrom TRU-Spec resin. The purified U–Th fraction was dissolved in 2% HNO_3 with addition of trace hydrofluoric acid and Brij-35 surfactant added to ensure complete dissolution of Th and to aid with sample nebulisation and wash-out. The dissolved samples were then introduced to the MC-ICP-MS where $^{234}U/^{238}U$ and $^{230}Th/^{238}U$ were measured from a single solution using a parallel ion-counting procedure. Results of the U–Th dating are

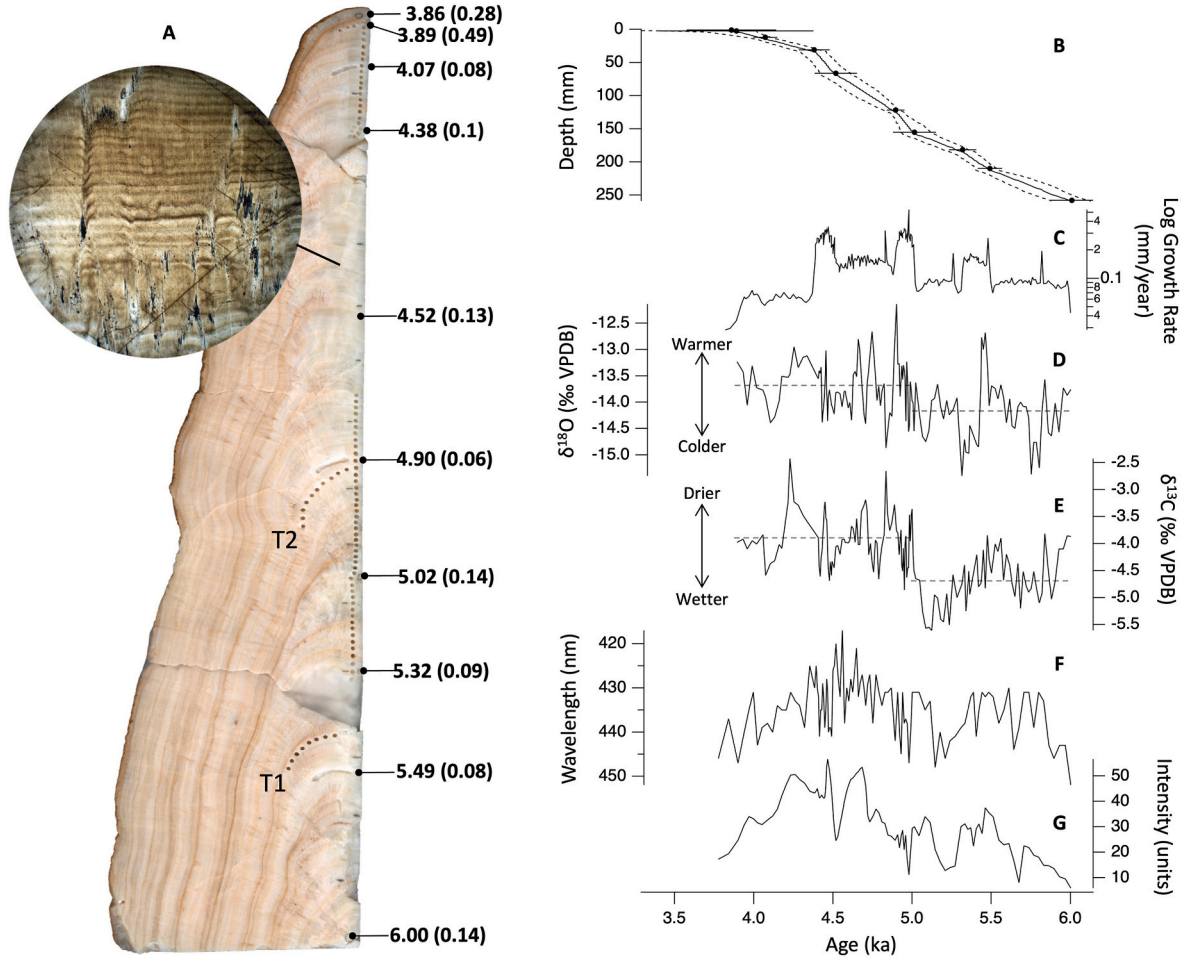

Fig. 2. Sample and results. A) TO1 stalagmite, with U–Th subsampling locations (black dots) and relative ages (in ka, uncertainties in bracket). Stable isotopes track is visible through the sampling holes, as well as the tested layers for Hendy Test (named T1 and T2). The rounded insert shows the main microfabric. B) TO1 age-depth model. Ages are reported with dots and 2σ error bars. Full line is the average model, while dotted lines represent ±2σ uncertainty propagation. C) TO1 growth rate, with log-scale. D-E) TO1$\delta^{13}C$- $\delta^{18}O$ timeseries; dotted lines represent the average value for the ~6 to ~5 and ~5 to ~3.8 ka periods. Arrows identify the main interpretation given to the proxies (see text). F-G) TO1 fluorescence wavelength and intensity.

presented in Table 1. Considering the detrital contamination, the ages were corrected for the effect of ^{230}Th by applying a $[^{230}Th/^{232}Th]_i$ of 0.65 ± 0.25, determined from stratigraphic constraints according to the methods described in Hellstrom (2006). Proxy time series were anchored in time using a Bayesian-Monte-Carlo-derived age model (see Drysdale et al., 2005). This model includes an uncertainty component that encompasses both spatial (introduced during sampling) and temporal domains arising from the corrected U–Th age determinations (Fig. 2). Ages are reported in ka (thousands of years before 1950 CE).

4. Results

TO1 consists entirely of porous, columnar calcite, with the porosity increasing toward the flanks of the speleothem. It shows visible alternation of lighter and darker growth layers with diffuse boundaries (Fig. 2).

All dated subsamples (Table 1) demonstrate a generally high concentration of ^{238}U (average = 205 ppb). Together with a moderate detrital Th concentration (average activity $^{230}/^{232}Th = 32$), this resulted in relatively low 2σ uncertainties associated with the final ages, which are mostly below 3%. The only exceptions are samples TO1-06 and TO1-05, where 2σ is 7.3% and 12.5% respectively. However, these latter are the most recent ages, where a relatively smaller production of authigenic ^{230}Th, with respect to older ages, is also responsible for larger uncertainties (Hua et al., 2012).

According to the age model, which has an average uncertainty of +80 and −90 years, the stalagmite was deposited between $6.00^{+0.13}/_{-0.12}$ and $3.82^{+0.19}/_{-0.53}$ ka (Fig. 2). Calcite deposition was continuous, with the possible exception of a short hiatus near the top. This is indicated by petrographic observations, but it cannot be constrained by the age model. Thus, we consider the duration of the hiatus to be within the age uncertainties associated with the model. The growth rate, from the bottom portion of the stalagmite to $4.4^{+0.06}/_{-0.09}$ ka, is around ~0.1 mm/year or greater. There are oscillations toward higher rates centered at $5.6^{+0.1}/_{-0.09}$ ka (~0.2 mm/year), and especially at $4.95^{+0.07}/_{-0.05}$ and $4.45^{+0.07}/_{-0.08}$ ka (both up to 0.35 mm/year). At $4.4^{+0.06}/_{-0.09}$ ka, the growth rate rapidly decreases to ~0.06 mm/year, and this lower rate is maintained until the top (Fig. 2).

Fig. 2 shows the $\delta^{13}C$ and $\delta^{18}O$ timeseries, with a final sampling resolution between 10 and 30 years. The $\delta^{18}O$ ranges from ca. −15 to −12‰, displaying the most evident high peaks at $5.45^{+0.07}/_{-0.08}$, $4.9^{+0.07}/_{-0.05}$, $4.75^{+0.08}/_{-0.1}$ and $4.25^{+0.08}/_{-0.08}$ ka. The lowest ratios are centered on $5.8^{+0.12}/_{-0.13}$ ka, $5.3^{+0.08}/_{-0.07}$, $5.1^{+0.09}/_{-0.09}$, $4.85^{+0.05}/_{-0.06}$, $4.5^{+0.1}/_{-0.08}$ and $4.1^{+0.08}/_{-0.07}$ ka. Several minor oscillations are superimposed to this peak-and-trough pattern. At multimillennial scale, it is noted that, on average, $\delta^{18}O$ is lower between ~6 and ~5 ka (−14.2 ± 0.6‰) compared to the period between ~5 and ~3.8 ka (−13.7 ± 0.5‰). $\delta^{13}C$ varies between −2.4 and −5.6‰; although correlation with $\delta^{18}O$ is weak ($r^2 = 0.11$, $p < 0.0001$, Cohen et al., 2013), the curves are to some extent similar at the multicentennial-millennial scale. This is

Table 1
Age data and sample depths for stalagmite TO1. The values are presented with 95% uncertainties. Isotope data are expressed as activity ratios. $^{230}Th/^{238}U$ is determined using a mixed spike calibrated against a solution of HU-1 - see Hellstrom (2003) for the detailed protocol. Age is calculated using the standard U–Th age equation, by decay constants of 9.195 × 10-6 and 2.835 × 10-6 for ^{230}Th and ^{234}U respectively. Corrected age is calculated allowing for an initial $^{230}Th/^{232}Th$ of 0.65 ± 0.25, included as an additional term in the standard U–Th age equation. $^{234}U/^{238}U(i)$ is calculated using $^{234}U/^{238}U$ and the corrected age.

Sample	Depth (mm)		^{238}U (ppb)			$^{230}Th/^{238}U$			$^{234}U/^{238}U$			$[^{232}Th/^{238}U] \times 10^3$			$^{230}Th/^{232}Th$	Age (Ka)			$^{234}U/^{238}U$ (i)			Age Corr (Ka)		
TO1-06	5.2	±	1	230	±	5	0.1338	±	0.0034	3,2809	±	0.006	31.1169	±	0.2174	4.3	4.507	±	0.116	3.3059	±	0.0063	3.859	±	0.283
TO1-05	6.7	±	1	200	±	4	0.15	±	0.002	3,2575	±	0.0066	56.6028	±	0.2941	2.7	5.101	±	0.069	3.2824	±	0.0073	3.891	±	0.485
TO1-9	17.1	±	1	184	±	14	0.1244	±	0.002	3,3103	±	0.0055	4.3111	±	0.0207	28.9	4.15	±	0.067	3.337	±	0.0055	4.073	±	0.076
TO1-02r	36.0	±	1	182	±	4	0.134	±	0.0023	3,2893	±	0.0085	6.4782	±	0.0359	20.7	4.503	±	0.077	3.3178	±	0.0086	4.382	±	0.097
TO1-10	71.6	±	1	–			0.1441	±	0.0016	3,3119	±	0.0065	14.8734	±	0.0322	9.7	4.814	±	0.052	3.3417	±	0.0066	4.518	±	0.134
TO1-8	127.0	±	1	159	±	12	0.1489	±	0.0014	3,3305	±	0.0058	3.4488	±	0.0835	43.2	4.95	±	0.046	3.363	±	0.0059	4.896	±	0.056
TO1-04	160.5	±	1	226	±	5	0.1535	±	0.0038	3,3268	±	0.0071	5.4534	±	0.0444	28.2	5.112	±	0.125	3.36	±	0.0072	5.015	±	0.136
TO1-03	186.7	±	1	212	±	4	0.163	±	0.0017	3,3129	±	0.0084	7.5061	±	0.0392	21.7	5.456	±	0.056	3.3479	±	0.0084	5.319	±	0.086
TO1-7	215.0	±	1	228	±	17	0.1642	±	0.0022	3,3103	±	0.0061	1.5101	±	0.0076	108.8	5.503	±	0.073	3.3464	±	0.0061	5.492	±	0.077
TO1-01r	260.2	±	1	226	±	7	0.1808	±	0.0038	3,3152	±	0.0093	3.6302	±	0.024	49.8	6.061	±	0.129	3.3549	±	0.0095	6.009	±	0.135

because some of the main $\delta^{13}C$ paths toward higher or lower values coincide with those in $\delta^{18}O$, as at around $5.45^{+0.07}/_{-0.08}$, $5.1^{+0.09}/_{-0.09}$ and $4.25^{+0.08}/_{-0.08}$ ka, although the main higher or lower peaks seldom coincide. Similarly to $\delta^{18}O$, at the multimillennial scale, the average $\delta^{13}C$ value appears lower between ~6 and ~5 ka (−4.7 ± 0.5‰) compared to the period between ~5 and ~3.8 ka (−3.9 ± 0.5‰). Finally, the two layers investigated for the Hendy test show that there is no convincing $\delta^{13}C$-$\delta^{18}O$ correlation along the laminae and $\delta^{18}O$ does not significantly increase from the axis toward the flank of the stalagmite (Fig. 3).

Fluorescence analyses (Fig. 2) reported a final resolution ranging between 16 and 48 years. Intensity increases from the bottom to $4.5^{+0.1}/_{-0.08}$ ka, shifting from almost 0 to 50 intensity units. Evident troughs are superimposed to this trend, centered at $5.65^{+0.11}/_{-0.1}$, $5.2^{+0.08}/_{-0.08}$, $5.0^{+0.11}/_{-0.07}$ and $4.5^{+0.1}/_{-0.08}$ ka. Importantly, these oscillations, producing increasing and decreasing trends, are coherent with those detected in $\delta^{13}C$ and $\delta^{18}O$. From ~4.5 ka to the top, the intensity decreases. Emission wavelength has the same pattern as intensity, but inverted. It shifts from 450 to 420 nm from the bottom to ~4.5 ka and then decreases at 430 nm until the top (Fig. 2).

5. Discussion

5.1. TO1-$\delta^{18}O$ as a paleotemperature proxy

When conditions for isotopic equilibrium prevail, the oxygen isotope composition of calcite speleothems primarily depends on drip water $\delta^{18}O$ and cave temperature at the time of $CaCO_3$ precipitation (McDermott, 2004). Kinetic effects are potentially present during speleothem deposition, and can affect both oxygen and carbon isotope composition to a variable extent (e.g. Mickler et al., 2006; Feng et al., 2012; Daëron et al., 2019). The outcome of the Hendy test (Hendy, 1971; Mickler et al., 2006) performed on TO1 and the lack of $\delta^{13}C$-$\delta^{18}O$ correlation along the vertical axis point to the absence of kinetic fractionation, although today the test is not considered as a definitive proof for isotopic equilibrium conditions (e.g. Dorale and Liu, 2009; Mühlinghaus et al., 2009; Day and Henderson, 2011). Low supersaturation rate, together with slow carbonate precipitation, might be the most suitable conditions for producing calcite close to equilibrium conditions (Daëron et al., 2019). In TO1, columnar calcite is the prevalent fabric, in turn generated by fluids with low $CaCO_3$ supersaturation levels at near-isotopic equilibrium conditions (Frisia et al., 2000). At the same time, growth rate is generally low (Fig. 2), and the homogeneous columnar fabric indicates a constant accretion throughout the year, with the crystal top surface constantly wet, rather than episodic - and more rapid – growth. Notwithstanding, in order to be as cautious as possible, the deposition of TO1 is here considered as having likely occurred at quasi-equilibrium conditions. This implies that variations in $\delta^{18}O$-$\delta^{13}C$ are predominantly due to climatic and environmental changes rather than driven by kinetic fractionation.

In the Siberian region, a high degree of correlation exists between surface temperature and the isotopic composition of rainfall precipitation (hereafter $\delta^{18}O_p$) (Kurita et al., 2004). In Enisejsk (250 km north from Krasnoyarsk), $\delta^{18}O_p$/T is ca. +0.4‰/°C (Fig. 1). Although the available data refer to one year only, the strong correlation ($r^2 = 0.88$, $p < 0.01$) still points to temperature as the main driver of $\delta^{18}O_p$ in the study area. In Western Siberia, $\delta^{18}O_p$/T has been defined at 0.5‰/°C for the last 50 years (Butzin et al., 2014), in a region ranging from 55 to 70°N and 55–90°E. Our study site is at the border of this region. However, in Irktusk, ca. 800 km south-east from Krasnoyarsk and close to Lake Baikal, the same 0.5‰/°C ($r^2 = 0.83$) gradient is found in a 6-year-long database (Kostrova et al., 2020). As this has been recommended for paleoclimate studies in this region (Kostrova et al., 2020), and the same has been applied to speleothem studies at Kyok-Tash Cave (ca. 750 km southwest from Krasnoyarsk, Li et al., 2021), we here also consider a $\delta^{18}O_p$/T relation of 0.5‰/°C for the further discussion. Additionally, the

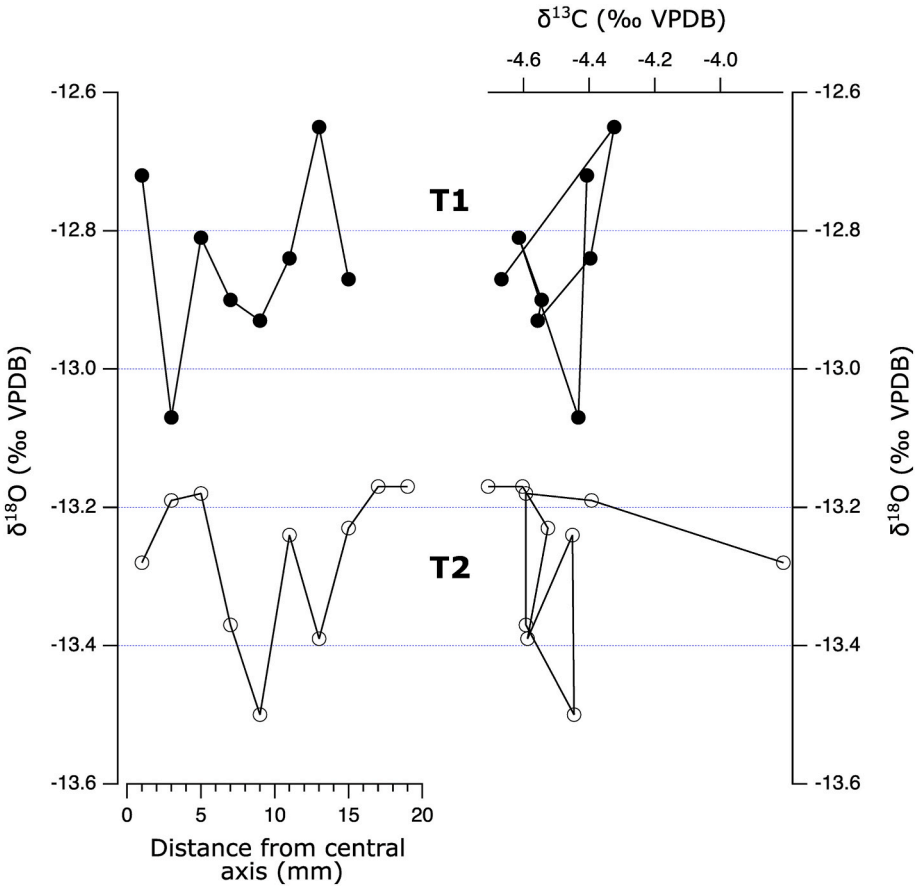

Fig. 3. The Hendy test. Tested layers are T1 and T2 (see Fig. 2 for locations).

Enisejsk meteorological station reveals a positive correlation ($r^2 = 0.59$, Fig. 1) between $\delta^{18}O_p$ and rainfall precipitation quantity, with a gradient of ca. 0.3‰/mm of rain (Fig. 1). However, the latter cannot be associated to the rainfall amount effect (Dansgaard, 1964) as this would produce a negative correlation due to rainout. Thus, the $\delta^{18}O_p$/rain amount correlation is possibly still related to the dominant effect of temperature, as summer is the wetter season in the study area. A similar interpretation was given in a recent compilation of $\delta^{18}O_p$ across Siberia and Central Asia (Wang et al., 2020).

We now assume that this signal is transmitted to the drip water feeding the Torgashinskaya Cave speleothems with minimal influence of kinetic processes. Furthermore, in-karst $CaCO_3$ supersaturation of the infiltrating water upstream of the cave chamber can produce prior calcite precipitation (PCP, Fairchild and Baker, 2012; Flohr et al., 2017), resulting in highly-correlated $\delta^{18}O$-$\delta^{13}C$ in TO1 record. However, the $\delta^{18}O$-$\delta^{13}C$ r^2-correlation along the central axis is 0.1 in TO1, excluding the occurrence of PCP. In any case, if acting during limited periods of time, PCP can only affect a portion of the stalagmite (Fairchild and Baker, 2012) producing for example contemporaneous short-lived high values in TO1 stalagmite, which anyway are not observed (with the exclusion of the $\delta^{18}O$-$\delta^{13}C$ simultaneous peak at ca. 5.7 ka). In this circumstance, shifts in $\delta^{18}O$ of calcite result from the arithmetic difference between the isotopic composition of the seepage and the water/-calcite fractionation factor in cave. The latter is also controlled by temperature, with a factor of −0.21‰/°C for in-situ farmed calcite (Tremaine et al., 2011). Considering that cave constant temperature throughout the year might represent the average annual temperature at the outside (De Waele and Gutiérrez, 2022), we should expect an increase of 0.5–0.21 = 0.29‰ in speleothem calcite $\delta^{18}O$ for 1 °C of average surface temperature increase, and *vice versa*. Therefore, assuming that these figures are valid for the mid to late Holocene, the $\delta^{18}O$ record would show a maximum range of temperature of ca. 10 °C. This appears a large estimate, but it is compatible for: 1) an area which shows annually a temperature range of 50 °C or more; and 2) $\delta^{18}O$ data in TO1 is not smoothed and the range of estimated temperature is also amplified considering the associated error in the isotopic measurements. However, the meaning of this temperature estimation is uncertain and largely depends on, for instance, the seasonal dynamics of water infiltration and calcite precipitation. For example, short-term changes in the seasonal distribution of precipitation, with rainfall more abundant during the warmer or colder months within the wet season, could likely enlarge the amplitude of $\delta^{18}O$ range. At the same time, the role of snow melt in recharging the karst aquifer cannot be excluded in modulating the $\delta^{18}O$ of the infiltration water. This is difficult to evaluate without long-term monitoring. Such information is, unfortunately, not available for this cave.

Thus, while we are rather confident that TO1 higher $\delta^{18}O$ values are reflecting warmer temperatures and *vice versa*, the calculated temperatures range needs to be treated with caution. From this perspective, the phases of lower $\delta^{18}O$ values indicate cooling at ca. ~5.8–5.7 ka, 5.4–5.3 ka, 5.1 ka, 4.8 ka, 4.4–4.6 and 4.1 ka. On the other hand, the main peaks of higher $\delta^{18}O$ values, at ~5.45, ~4.9, ~4.75 and ~4.25 ka indicate higher temperatures. Additionally, the period from ~5 to ~3.8 ka, where average $\delta^{18}O$ values are slightly more positive (ca. 0.5‰) than the previous period from ca. 6 to 5 ka, suggest differences in the average temperature of approximately 1.8 °C.

5.2. *$\delta^{13}C$ and fluorescence as paleoenvironmental indicators*

Understanding the relationship between variations in speleothem calcite $\delta^{13}C$ and climate is often elusive because of the complex epikarst processes involved (Fairchild and Baker, 2012; Mühlinghaus et al.,

2009; Dreybrodt and Scholz, 2011; Fohlmeister et al., 2020 and references therein), variable proportions of soil derived (biogenic) and rock-derived carbon (Genty et al., 1999; Rudzka et al., 2011), changes in soil CO_2-productivity and type of vegetation (e.g. Lechleitner et al., 2021). Additionally, the relation between water residence time in soil and its equilibration with soil CO_2 can be important (e.g. Bar-Matthews et al., 1996), as can PCP (e.g. Stoll et al., 2022). Studies of the ^{14}C systematics in speleothems have demonstrated that also the relative proportion of old stored and more recalcitrant carbon *versus* labile components of soil organic matter decomposition can also be important in defining the final carbon isotope composition during climate change (Rudzka et al., 2011; Noronha et al., 2014).

However, in temperate settings, prominent shifts towards higher $\delta^{13}C$ values are usually interpreted to correspond to phases of climatic deterioration reducing soil CO_2 productivity (Pérez-Mejías et al., 2019; Columbu et al., 2022) possibly accompanied by changes in the amount of oxidation of different carbon compounds in soil organic matter and/or increased contribution of dissolved limestone (Rudzka et al., 2011; Noronha et al., 2014). Also, reduction in cave recharge, enhancing PCP (e.g. Baker et al., 1997; Drysdale et al., 2006) or favoring limestone dissolution by pyrite oxidation, (Spötl and Mangini, 2007; Piccini et al., 2008), can enrich in the heavy isotope the $\delta^{13}C$ of speleothem calcite. Therefore, increasing $\delta^{13}C$ values are usually interpreted as drier/colder conditions (e.g. Genty et al., 2003; Drysdale et al., 2006) and changes to lower values as due to wetter/warmer climate conditions, related to the soil bioproductivity (e.g. Fohlmeister et al., 2020; Lechleitner et al., 2021). This has also been proposed for high-latitude (Sundqvist et al., 2010) and high-altitude speleothems (Columbu et al., 2018), as well as for desert-like environments (Columbu et al., 2022). Notwithstanding this, there are also divergent interpretations. For instance, at Moaning Cave (Sierra Nevada), lower $\delta^{13}C$ values have been related to the cold-wet conditions during the Late Glacial, which encouraged more soil activity (Oster et al., 2009).

For TO1, the primary influence of PCP in modulating $\delta^{13}C$ can be excluded as explained above. Additionally, there is no evidence to invoke limestone dissolution as governed by pyrite oxidation rather than CO_2 from soils, as this would produce speleothem $\delta^{13}C$ ratios with values around or above 0‰ (Bajo et al., 2017). Finally, it is difficult to argue that $\delta^{13}C$ in TO1 is driven by evaporative phenomena during the deposition of the stalagmite, as the low temperature and high humidity in the studied cave are already against this process. Moreover, evaporation would not have produced columnar calcite (Frisia et al., 2011) and $\delta^{13}C$-$\delta^{18}O$ would have been strongly correlated - also responding to evaporation-controlled kinetic deposition of $CaCO_3$ (Fairchild and Baker, 2012). Thus, we consider here TO1-$\delta^{13}C$ as indicator of biogenic CO_2 production in soils above the cave during the deposition of the speleothem. TO1-$\delta^{13}C$ negative values are those produced in speleothems by C4-dominated vegetation at the surface (ranging from −6.0 to −2.0‰ (McDermott, 2004)), suggesting that soils bioactivity as well as CO_2 inputs from old organic matter might have played a role here (Bajo et al., 2017).

In TO1, $\delta^{13}C$ average values are higher by ca.1.3‰ in the period between ~5 and ~3.8 ka, compared to the previous ~6 to 5 ka period. During the same interval, $\delta^{18}O$ points toward higher temperatures. This would indicate that lower soil bioproductivity, associated to drier conditions, occurred during the period of warmer temperatures. Conversely, lower temperatures favored a wetter climate. Thus, $\delta^{13}C$ in TO1 shift would be better explained by a period of cooler and wetter conditions from ca. 5 to 6 ka, whereas warmer but drier conditions seem to persist between ca. 5 and 3.8 ka (Fig. 2).

Notwithstanding the above, not all $\delta^{18}O$ oscillations are matched by similar changes in $\delta^{13}C$. Soil response time might have a role here. For instance, during rapid and low-amplitude temperature variations, there is no significant change in soil CO_2 productivity. Most importantly, in continental climates, the role of seasonality is particularly important in defining the processes of mineralization of organic matter, and so seasonal changes in temperature and precipitation control soil organic matter turnover and decomposition of recalcitrant *versus* labile soil organic matter, and subsequently the amount of soil CO_2 and its isotopic composition. Indeed, the decomposition of different fractions of soil organic matter is dependent on temperature, with some evidence for more recalcitrant organic matter being effectively decomposed as temperature increases (Leifeld and Fuhrer, 2005; Knorr et al., 2005).

It is counter-intuitive that biogenic CO_2 production will increase during colder climates causing stalagmite $\delta^{13}C$ to become more negative, given the overall global relationship between soil CO_2 production and temperature (e.g. Raich and Schlesinger, 1992), and the correlation of soil CO_2 with rainfall amount and mean annual evapotranspiration (Brook et al., 1983). A dependence of the carbon isotopic composition of ecosystem respiration on plant and soil organic matter and the amount of precipitation has been observed by Bowling et al. (2001), who reported higher $\delta^{13}C$ in the driest localities. Notwithstanding, long-term snow cover on forest can enhance CO_2 accumulation into the soil, which can then be flushed into the cave at times of snow melting (Solomon and Cerling, 1987). Snow cover is also important due to its insulation capacity for maintaining the temperature of the soil above freezing, which affects CO_2 production during winter (Mariko et al., 2000). It is important to note that boreal forest CO_2 production is strongly reduced during winter, being dominated by microbial activity instead of root respiration (Groffman et al., 2006). Measurement of radiocarbon ($\Delta^{14}C$) suggests that winter CO_2 production may result from mineralization of older organic matter stored in the soil (Winston et al., 1997). The amount of CO_2 produced during winter can account for up to ca. 20% of the total soil CO_2 produced (Winston et al., 1997). Therefore, the amount of winter-to-summer CO_2 production is effectively controlled by the dynamics of the two seasons, such as length, relative temperatures, snow cover, etc. Consequently, an important amount of soil CO_2 can be flushed into the karst after a long winter accumulation favored by longer snow cover (the insulation effect), and an additional important amount can be added during a wet summer. Although this "dual CO_2" effect can lead to different isotopic compositions (microbial *versus* plant root respiration), the amount of soil CO_2 would be greater when the winter is longer and summer is wetter. This can have the effect of making the $\delta^{13}C$ of speleothem calcite more negative during cooler but wetter conditions, while warmer but drier periods drive $\delta^{13}C$ towards less negative values. Therefore, higher $\delta^{13}C$ values of speleothem calcite during warmer periods are plausible in cold regions if accompanied by drier conditions (and *vice versa*), and this can differentiate Siberia from areas with milder and less continental climates.

Fluorescence data might support this interpretation. Organic matter is incorporated into speleothems via several processes (Pearson et al., 2020 and references therein), with the overlying soils constituting the main source (Perrette et al., 2015; Blyth et al., 2016). A portion of organic matter trapped in speleothems fluoresces (Aiken, 2014), so changes in calcite fluorescence properties can reflect variations in dissolved organic matter released from the soil (McGarry and Baker, 2000; Borsato et al., 2007; Hartland et al., 2010; Pearson et al., 2020; Endres et al., 2023). This is related to the humification process, which drives the decomposition of organics by microbial activity (Hille, 2004) and thus the content of organic polymers in pedogenic layers. Infiltrating waters transport the compounds produced by humification to the cave system, where they are embedded into the calcite. At higher rainfall and/or colder temperature, humification is limited because compounds are flushed rapidly from soils for the first, while microbial activity is relatively low for the second factor (Swift et al., 1979). Calcite in the cave would thus incorporate organics that fluoresce at significantly longer peak emission wavelengths. In contrast, with lower rainfall and/or warmer conditions, humification is more advanced, with the calcite-bound compounds fluorescing at shorter emission wavelengths (McGarry and Baker, 2000). Instead, luminescence intensity depends on different factors (Shapov et al., 1994; Baker et al., 1996; McGarry and Baker, 2000). Considering a single stalagmite fed by the same drip, such

factors include: i) the presence of substances with different degrees of humification, with more humified substances having higher luminescence intensity; ii) the drip rate; iii) changes in speleothem growth rate. Other processes have been documented as drivers of fluorescence wavelength and intensity variations in speleothems, such as microbial activity in the karst network and the cave environment, water residence time, and the flow-path length and/or compounds sourced from the bed rock (Blyth et al., 2016; Pearson et al., 2020). Unfortunately, the absence of monitoring data inhibits our ability to resolve further mechanisms controlling the fluorescence properties in this study case. We instead noticed that higher fluorescence intensities (albeit with a pronounced trough) are notable from 4.7 to 4.2 ka (Fig. 2) and generally correspond to shorter emission wavelengths. Accordingly, the speleothem fluorescence in this interval appears to reflect the infiltration of more humified soil organic compounds, suggesting a drier but warmer climate, in agreement with the carbonate $\delta^{13}C$ data. Despite the inferred

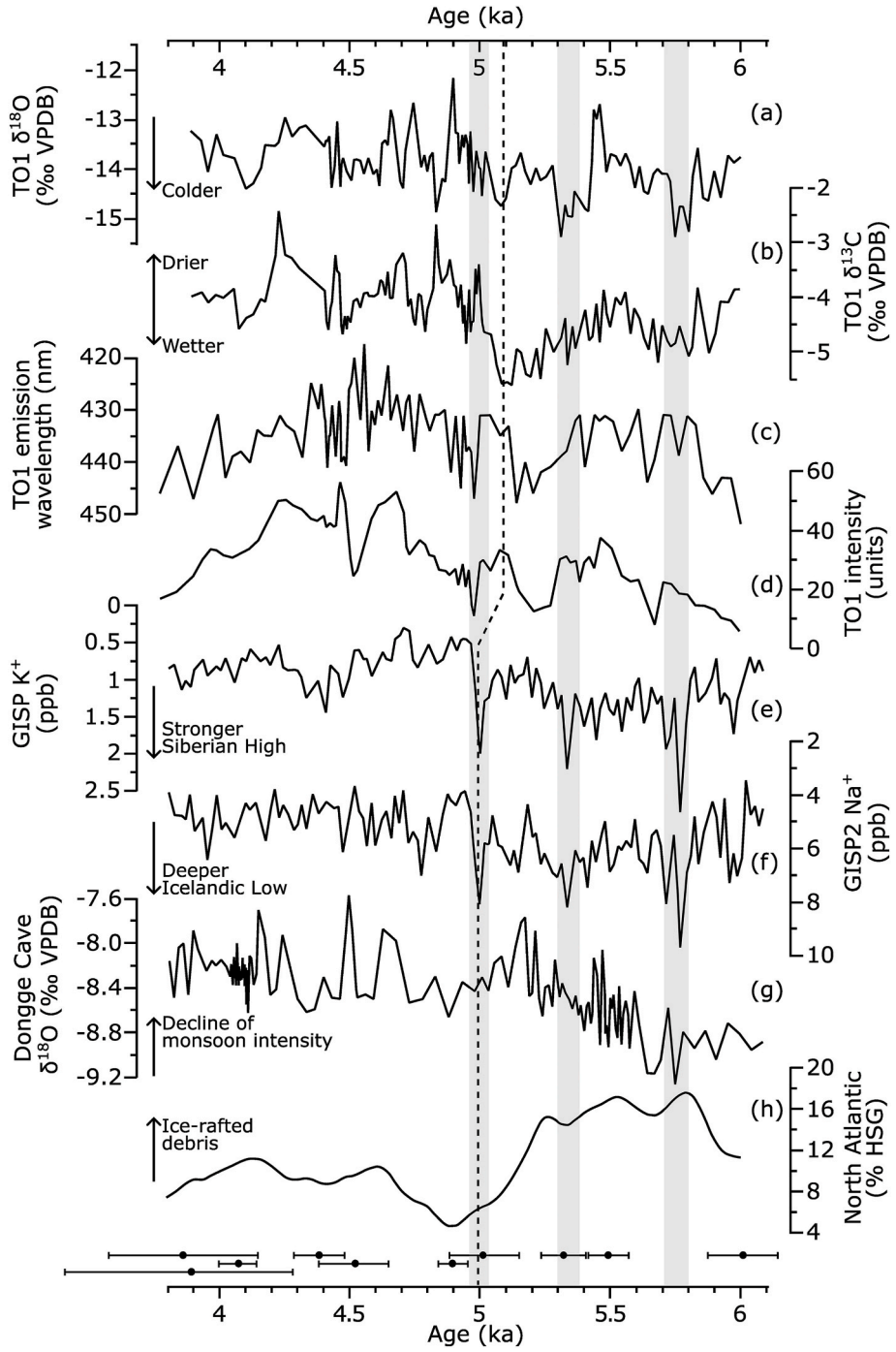

Fig. 4. Comparison between TO1 and Northern Hemisphere records. (A) TO1 $\delta^{18}O$, proxy of temperature. (B) TO1 $\delta^{13}C$, proxy of rainfall. (C–D) TO1 fluorescence properties: emission wavelength (nm) and intensity (units), proxies for temperature and soil humidity. (e) GISP K^+ (ppb) proxy for the Siberian high intensity (Mayewski et al., 1997). (F) GISP Na^+, proxy for the Iceland low intensity (Mayewski et al., 1997); (G) Dongge Cave stalagmite $\delta^{18}O$ (Dykoski et al., 2005), proxy for the Asian monsoon intensity. (H) North Atlantic Hematite-stained grains, proxy for the Holocene ice raft events (Bond et al., 2001). Grey bands indicate the timing of significant intensification of Siberian High as taken from GISP K^+ database. The shift observed between TO1 and GISP (dotted line), is within 2σ uncertainties of both records. On the bottom, dots and error bars refer to U–Th ages from TO1 record.

drier conditions, there is no compelling case for a significant reduction in water discharge to the speleothem, because the growth rate is rather constant and it only decreases at around 4.4 ka (Fig. 2). This may be due to the hydrological pathway that the percolation waters take through the vadose zone *en route* to the cave. There is a certain delay between the increasing intensity and decreasing wavelength signal at ca. 4.7 ka and the calcite $\delta^{13}C$ shifts occurring at ca. 5 ka. This can in part be due to the averaging effects of the relatively large (4.5 mm diameter) spot size of the fibre-optic probe used in the fluorescence measurements, but might also suggest that soil organic matter compounds respond slightly differently in time compared to the $\delta^{13}C$ of drip solution.

5.3. Paleoclimate reconstruction

TO1 $\delta^{13}C$-$\delta^{18}O$ and fluorescence proxies suggest that the period from ca. 5 to 3.8 ka (or more strictly speaking, following the fluorescence

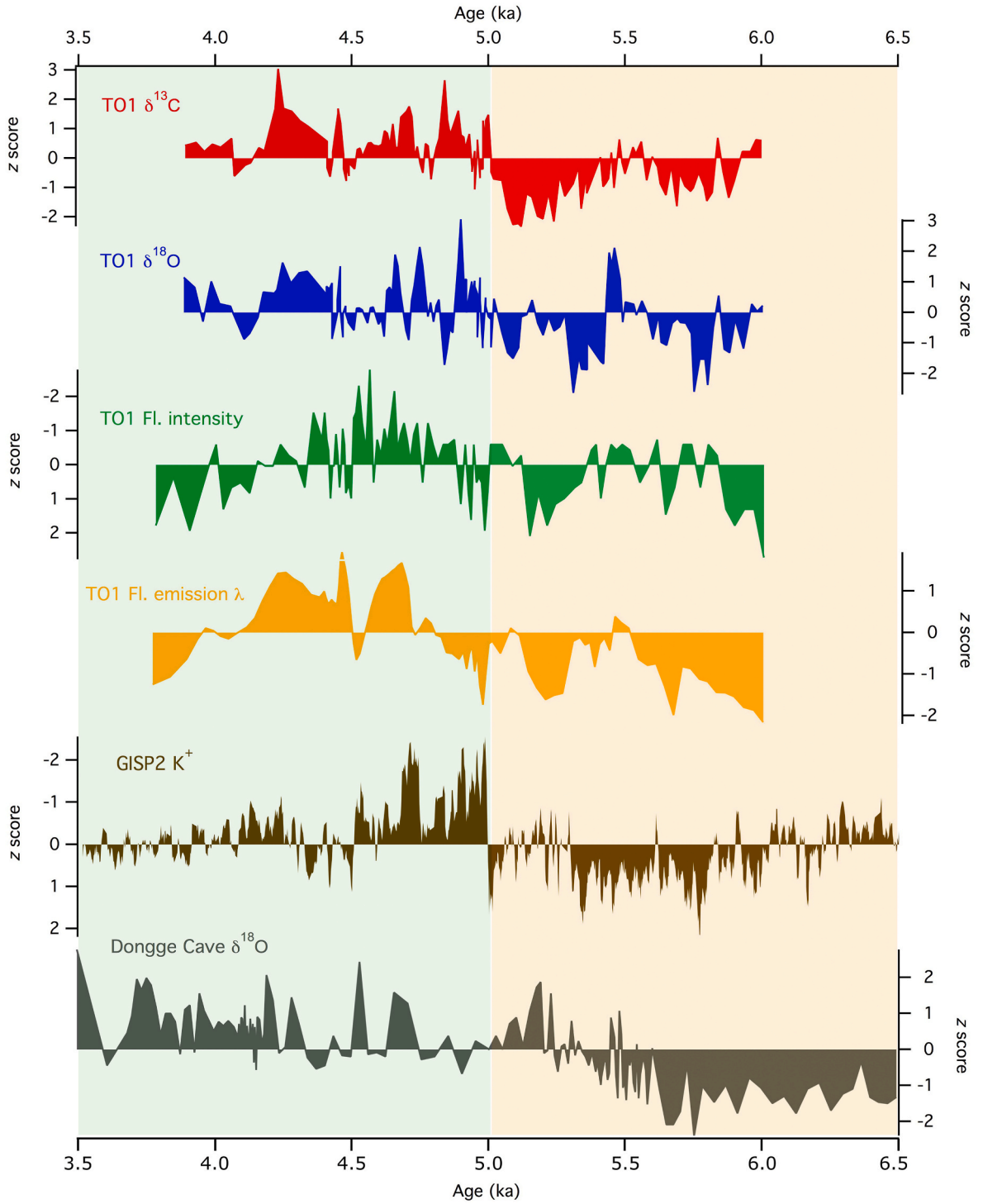

Fig. 5. z-scores comparison between TO1 and Northern Hemisphere records. From top to bottom, z-scores are reported for TO1 $\delta^{13}C$, $\delta^{18}O$, fluorescence intensity and fluorescence emission wavelength (this study); then GISP K^+ (Mayewski et al., 1997) and Dongge Cave $\delta^{18}O$ (Dykoski et al., 2005). It is evident the shift in paleoclimate-environmental conditions occurring in the period between ~5 and ~3.8 ka (green shading), compared to the previous ~6 to 5 ka period (orange shading).

timeseries, from ca. 5 to 4.2 ka) is characterized by slightly warmer and drier conditions relative to the previous period from ca. 6 to 5 ka. The increase of growth rate at ca. 5 ka (Fig. 2) supports the occurrence of important environmental changes. According to the proposed interpretation, the increase in growth rate indicates an increase in temperature, rather than an increase in precipitation. The conical shape of the stalagmite may support a progressive reduction in water supply towards the top, although the same effect can also be produced by the senescence of the karst fracture network feeding the speleothem (Martín-Chivelet et al., 2017).

Regional palaeoclimate proxy data agree with the inferences derived from speleothem TO1. Quantitative reconstruction of Holocene vegetation and climate dynamics in the semiarid Mongolian Altai from Hoton-Nur Lake (Rudaya et al., 2009) indicates that boreal woodland replaced the open landscape of northwestern Mongolia at about 10 ka, in response to a remarkable increase in precipitation from 200 to 250 mm/yr to 450–550 mm/yr. A decline in forest vegetation and a return to a predominance of open vegetation occurred after 5 ka, when precipitation decreased to 250–300 mm/yr. The diatom $\delta^{18}O$ record from Lake Baikal, although discontinuous for the period of interest, shows a sharp $\delta^{18}O$ shift at ca. 5 ka suggesting a transition from colder to warmer conditions (Morley et al., 2005). Interestingly, this transition is well marked by changes in diatom concentrations, suggesting important paleolimnological changes. Records of K^+ and Na^+ in Greenland ice cores are respectively applied as proxies for intensity of the SH and IL (Mayewski et al., 1997; Meeker and Mayewsky, 2002, Fig. 4). Considering the long-term trend, there is a clear step in the concentration of K^+ and Na^+ in Greenland ice cores at ca. 5 ka, which indicates a reduction of the intensity of SH and IL, occurring within a century or two of the most important changes in stable isotope ratios and fluorescence properties of the TO1 record. The same is evident by evaluating the z-scores (Fig. 5). The reduction of SH intensity may have produced less severe and shorter winters, with less snow precipitation in the area accompanied with longer, warmer and drier summer conditions. At ca. 5 ka there is a substantial reduction in ice-rafted debris in subpolar cores (Fig. 4, Bond et al., 2001), indicating that the polar front regionally moved northward. Over essentially the same period, the isotopic composition of Dongge cave speleothems (Figs. 4 and 5, Dykoski et al., 2005) in southern China shows a progressive decrease in monsoon intensity from ca. 5.2 ka. In the Chinese speleothem, calcite $\delta^{18}O$ is usually interpreted as a proxy for the strength of the Summer Monsoon (Wang et al., 2001; Yuan et al., 2004) and the trend reported for Dongge is consistent with a reduction of monsoon intensity.

In contrast to the interpretation proposed here, analyses from a peat core retrieved nearby Krasnojarsk recently suggested more humid conditions in the area since at least 5.2 ka, persisting until ca. 1.5 ka (Mikhailova et al., 2021). This interpretation is mostly based on the presence of a ca. 50 cm thick silt deposit, attributed to fluvial flooding. Unfortunately, the poor chronological constraint in the peat record prevents comparison with the TO1 timeseries. However, we believe that the two records could be still concordant considering that: 1) the silt deposit could have been the result of sporadic flooding rather than a prolonged multimillennial wetter period; or 2) the claimed wetter period commences after 4 ka (i.e. when the peak of drier conditions is terminated in TO1), but the low chronological resolution of the peat core record is unable to define this boundary. This is because the peat record has one highly uncertainty cal. age at ca. 5 ka followed by another at ca. 2 ka, while TO1 is presenting seven U–Th ages between ca. 5 and 3.8 ka.

Other short events, characterized in particular by lower $\delta^{18}O$, are also evident in TO1. Significantly, the isotopic excursions at ca. 5.8, 5.3 and 5.1 ka concur (within age error) with higher concentrations of K^+ (Fig. 5), in agreement with the interpretation that they represent cooling phases associated with more intense SH. This supports the notion that $\delta^{18}O$ in TO1 record may be sensitive to the strength of the SH. Climatic cooling at around ca. 5.1 and 5.3 ka has also been identified in other archives in the Northern Hemisphere, in particular around the European Alps and the circum-Mediterranean area (e.g. Magny and Haas, 2004; Staubwasser and Weiss, 2004; Zanchetta et al., 2014). Their precise correlation is, however, problematic and further discussion would be speculative.

Correlation between TO1 and Greenland proxies for shorter events is less clear for the period between ca. 3.8 and 5 ka. However, the $\delta^{18}O$ sudden decrease centered at 4.1 ka, pointing toward colder temperatures, occurred during a period of lower growth rate, increased fluorescence emission wavelength and decreased intensity (Figs. 2 and 4). This broadly corresponds to the cold/dry "4.2 event", identified in other records in the Northern Hemisphere (Weiss et al., 1993; Bond et al., 2001; Drysdale et al., 2006; Magny et al., 2009; Zanchetta et al., 2016, 2019; Liu and Feng, 2012; Bini et al., 2019; Isola et al., 2019; Giesche et al., 2023). However, this event is spatially complex and poorly expressed in northwest Eurasia (Roland et al., 2014) and its presence in some regions is under discussion (Bini et al., 2019 and reference therein).

6. Conclusions

The multiproxy record (stable isotope ratios and fluorescence properties) from stalagmite TO1 supports a shift from colder and wetter conditions between ca. 6 and 5 ka to warmer and drier conditions between ca. 5 and 3.8 ka. At around ca. 5 ka important changes occur both regionally and hemispherically, related to the so-called 'middle-late Holocene transition'. In particular, the comparison with Greenland suggest that this climate transition is accompanied by variations in ice properties that are sensitive to the intensity of SH (K^+) and IL (Na^+), in agreement with the proposed climatic reconstruction for the TO1 record. This also corresponds to a reduction of of ice-rafted debris deposition in subpolar cores from the North Atlantic. At around this time, summer Asian monsoon intensity also shows a reduction.

Several shorter cooling events are also present in TO1, notably at 5.8, 5.3 and 5.1 ka, and match (within the age errors) the K^+ and Na^+ records in Greenland ice cores. This study highlights that speleothem chemical-physical characteristics are key proxies for identifying changes in SH intensity and their local effects on moisture, temperature and soil processes.

Author contributions

All authors made a substantial contribution to the submission and that all authors approved the final version of the manuscript. In particular, GZ and LVZ conceived the paper, analyzed the data and wrote the first version of the manuscript. AC reanalysed the data and rewrote the text, with inputs from all authors. Geochemical analyses and/or sample preparation were accomplished by LVZ, JCH, II, ER and AEF. AC, GZ, TF and RD reviewed the manuscript after the reviewers' comments.

Declaration of competing interest

The authors declare that they have no known competing financial interests or personal relationships that could have appeared to influence the work reported in this paper.

Data availability

Data will be made available on request.

Acknowledgements

This research has been funded by University of Pisa (Fondi di Ateneo, G. Zanchetta); SUERC was supported by NERC and a consortium of Scottish Universities. We are grateful to two anonymous reviewers for their comments and useful suggestions.

References

Aiken, G.R., 2014. Fluorescence and Dissolved Organic Matter: A Chemist's Perspective. Cambridge University Press.

Ait Brahim, Y., Wassenburg, J.A., Sha, L., Cruz, F.W., Deininger, M., Sifeddine, A., Bouchaou, L., Spötl, C., Edwards, R.L., Cheng, H., 2019. North Atlantic ice–rafting, ocean and atmospheric circulation during the Holocene: insights from Western Mediterranean speleothems. Geophys. Res. Lett. 46, 7614–7623.

Bajo, P., Borsato, A., Drysdale, R., Hua, Q., Frisia, S., Zanchetta, G., Hellstrom, J., Woodhead, J., 2017. Stalagmite carbon isotopes and dead carbon proportion (DCP) in a near-closed-system situation: an interplay between sulphuric and carbonic acid dissolution. Geochem. Cosmochim. Acta 210, 208–227.

Baker, A., Barnes, W.L., Smart, P.L., 1996. Speleothem luminescence intensity and spectral characteristic: signal calibration and a record of paleovegetational change. Chem. Geol. 130, 65–70.

Baker, A., Ito, E., Smart, P.L., McEwan, R.F., 1997. Elevated and variable values of $\delta^{13}C$ in speleothems in a British cave system. Chem. Geol. 136, 263–270.

Bar-Matthews, M., Ayalon, A., Matthews, A., Sass, E., Halicz, L., 1996. Carbon and oxygen isotope study of the active water-carbonate system in a karstic Mediterranean cave: implications for paleoclimate research in semiarid regions. Geochem. Cosmochim. Acta 60, 337–347.

Berstad, I.M., Lundberg, J., Lauritzen, S.-E., Linge, H.C., 2002. Comparison of the climate during marine isotope stage 9 and 11 inferred from a speleothem isotope record from northern Norway. Quat. Res. 58, 361–371.

Bini, M., Zanchetta, G., Perşoiu, A., Cartier, R., Català, A., Cacho, I., Dean, J.R., Di Rita, F., Drysdale, R.N., Finnè, M., Isola, I., 2019. The 4.2 ka BP Event in the Mediterranean region: an overview. Clim. Past 15, 555–577.

Blyth, A.J., Hartland, A., Baker, A., 2016. Organic proxies in speleothems – new developments, advantages and limitations. Quat. Sci. Rev. 149, 1–17.

Bond, G., Kromer, B., Beer, J., Muschler, R., Evans, M.N., Showers, W., Hoffmann, S., Lotti-Bond, R., Hajdas, I., Bonani, G., 2001. Persistent solar influence on North Atlantic climate during the Holocene. Science 294, 2130–2136.

Borsato, A., Frisia, S., Fairchild, I.J., Somogyi, A., Susini, J., 2007. Trace element distribution in annual stalagmite laminae mapped by micrometer-resolution X-ray fluorescence: implications for incorporation of environmentally significant species. Geochem. Cosmochim. Acta 71, 1494e1512.

Bowling, D.R., McDowell, N.G., Bond, B.J., Law, B.E., Ehleringer, J.R., 2001. ^{13}C content of ecosystem respiration is linked to precipitation and vapor pressure deficit. Oecologia 131, 113–124.

Butzin, M., Werner, M., Masson-Delmotte, V., Risi, C., Frankenberg, C., Gribanov, K., Jouzel, J., Zakharov, V.I., 2014. Variations of oxygen-18 in West Siberian precipitation during the last 50 years. Atmos. Chem. Phys. 14, 5853–5869.

Cheng, H., Spötl, C., Breitenbach, S.F., Sinha, A., Wassenburg, J.A., Jochum, K.P., Scholz, D., Li, X., Yi, L., Peng, Y., Lv, Y., 2016. Climate variations of Central Asia on orbital to millennial timescales. Sci. Rep. 6, 36975.

Cohen, J., Saio, K., Enekhabi, D., 2001. The role of the Siberian High in Northern Hemisphere climate variability. Geophys. Res. Lett. 28, 299–302.

Cohen, L., Jarvis, P., Fowler, J., 2013. Practical Statistics for Field Biology. John Wiley & Sons.

Columbu, A., Sauro, F., Lundberg, J., Drysdale, R., De Waele, J., 2018. Palaeoenvironmental changes recorded by speleothems of the southern Alps (Piani Eterni, Belluno, Italy) during four interglacial to glacial climate transitions. Quat. Sci. Rev. 197, 319–335.

Columbu, A., Gazquez, F., Corrick, E., Hellstrom, J., Cheng, Drysdale R., 2022. Environmental changes in Sorbas arid region (Southern Spain) during MIS 5a inferred from a carbonate flowstone from a gypsum cave. Palaeogeogr. Palaeoclimatol. Palaeoecol. 607, 111275.

Daëron, M., Drysdale, R.N., Peral, M., Huyghe, D., Blamart, D., Coplen, T.B., Lartaud, F., Zanchetta, G., 2019. Most Earth-surface calcites precipitate out of isotopic equilibrium. Nat. Commun. 10, 429.

Dansgaard, W., 1964. Stable isotopes in precipitation. Tellus 16, 436–468.

Day, C.C., Henderson, G.M., 2011. Oxygen isotopes in calcite grown under cave-analogue conditions. Geochem. Cosmochim. Acta 75, 3956–3972.

De Waele, J., Gutiérrez, F., 2022. Karst Hydrogeology, Geomorphology and Caves. John Wiley & Sons.

Debret, M., Sebag, D., Crosta, X., et al., 2009. Evidence from wavelet analysis for a mid-Holocene transition in global climate forcing. Quat. Sci. Rev. 28, 2675–2688.

Della Libera, M.E., Novello, V.F., Cruz, F.W., Orrison, R., Vuille, M., Maezumi, S.Y., de Souza, J., Cauhy, J., Campos, J., Ampuero, A., Utida, G., 2022. Paleoclimatic and paleoenvironmental changes in Amazonian lowlands over the last three millennia. Quat. Sci. Rev. 279, 107383.

Dong, X., Kathayat, G., Rasmussen, S., Svensson, A., Severinghaus, J., Li, H., Yao, Xu1, Baker, J., Cai, Y., Zhang, H., Pérez-Mejías, C., Zhao, J., Spötl, C., Columbu, A., Ning, Y., Sinha, A., Stríkis, N., Chen, S., Wang, X., Gupta, A., Dutt, S., Zhang, F., Cruz, F., An, Z., Edwards, L., Cheng, H., 2022. Coupled atmosphere-ice-ocean dynamics during heinrich Stadial 2. Nat. Commun. 13, 867.

Dorale, J.A., Liu, Z.B., 2009. Limitations of Hendy test criteria in judging the paleoclimatic suitability of speleothems and the need for replication. J. Cave Karst Stud. 71, 73–80.

Dreybrodt, W., Scholz, D., 2011. Climatic dependence of stable carbon and oxygen isotope signals recorded in speleothems; from soil water to speleothem calcite. Geochem. Cosmochim. Acta 75, 734–752.

Drysdale, R.N., Zanchetta, G., Hellstrom, J.C., Fallick, A.E., Zhao, J-x, 2005. Stalagmite evidence for the onset of the Last Interglacial in southern Europe at 129 ka. Geophys. Res. Lett. 32, L24708.

Drysdale, R.N., Zanchetta, G., Hellstrom, J.C., Maas, R., Fallick, A.E., Pickett, M., Cartwright, I., Piccini, L., 2006. Late Holocene drought responsible for the collapse of Old World civilizations is recorded in an Italian cave flowstone. Geology 34, 101–104.

Dykoski, C.A., Edwards, L.E., Cheng, H., Yuan, D., Cai, Y., Zhang, M., Lin, Y., Qing, J., An, Z., Revenaugh, J., 2005. A high-resolution, absolute-dated Holocene and deglacial Asian monsoon record from Dongge Cave, China. Earth Planet Sci. Lett. 233, 71–86.

Endres, L., Jacquin, C., Gonzáles-Lemos, S., Rodríguez-Rodríguez, L., Sliwinski, J., Kaushal, N., Kost, O., Stoll, H., 2023. Climatic and cave settings influence on drip water fluorescent organic matter with implications for fluorescent laminations in stalagmites. Quat. Res. Accepted.

Fairchild, I.J., Baker, A., 2012. Speleothem Science. From Processes to Past Environments. Wiley-Blackwell, p. 432.

Fairchild, I.J., Claire, L., Smith, C.L., Baker, A., Fuller, L., Spötl, C., Mattey, D., McDermott, F., E I, M.F., 2006. Modification and preservation of environmental signals in speleothems. Earth Sci. Rev. 75, 105–153.

Feng, W., Banner, J., Guilfoyle, A., Musgrove, M., James, E., 2012. Oxygen isotopic fractionation between drip water and speleothem calcite: a 10-year monitoring study, central Texas, USA. Chem. Geol. 304–305, 53–67.

Fletcher, W.F., Debret, M., Sanchez-Goñi, M.F., 2013. Mid-Holocene emergence of a low-frequency millennial oscillation in western Mediterranean climate: implications for past dynamics of the North Atlantic atmospheric westerlies. Holocene 23, 153–166.

Flohr, P., Fleitmann, D., Zorita, E., Sadekov, A., Cheng, H., Bosomworth, M., Edwards, L., Matthews, W., Matthews, R., 2017. Late Holocene droughts in the Fertile Crescent recorded in a speleothem from northern Iraq. Geophys. Res. Lett. 16, 1528–1536.

Fohlmeister, J., Voarintsoa, N.R.G., Lechleitner, F.A., Boyd, M., Jacobson, M.J., Oster, J. L., 2020. Main controls on the stable carbon isotope composition of speleothems. Geochem. Cosmochim. Acta 279, 67–87.

Fohlmeister, J., Sekhon, N., Columbu, A., Vettoretti, G., Weitzel, N., Rehfeld, K., Veiga-Pires, C., Marwan, N., Boers, N., 2023. Global reorganization of atmospheric circulation during Dansgaard-Oeschger cycles. Proc. Natl. Acad. Sci. USA 120, e2302283120.

Frisia, S., Borsato, A., Fairchild, I., McDermott, F., 2000. Calcite fabrics, growth mechanisms, and environments of formation in speleothems from the Italian Alps and southwestern Ireland. J. Sediment. Petrol. 70, 1183–1196.

Frisia, S., Borsato, A., Fairchild, I., Fohlmeister, J., Miorandi, R., Spötl, C., 2011. Carbon mass-balance modelling and carbon isotope exchange processes in dynamic caves. Geochem. Cosmochim. Acta 75, 380–400.

Frisia, S., 2015. Microstratigraphic logging of calcite fabrics in speleothems as tool for palaeoclimate studies. Int. J. Speleol. 40, 1–16.

Genty, D., Massault, M., Gilmour, M., Baker, A., Verheyden, S., Keppens, E., 1999. Calculation of past dead carbon proportion and variability by the comparison of AMS ^{14}C and TIMS U/Th ages on two Holocene stalagmites. Radiocarbon 4, 251–270.

Genty, D., Blamart, D., Ouahdi, R., Gilmour, M., Baker, A., Jouzel, J., Van-Exter, S., 2003. Precise dating of Dansgaard-Oeschger climate oscillations in western Europe from stalagmite data. Nature 421, 833–837.

Giesche, A., Hodell, D.A., Petrie, C.A., Haug, G.H., Adkins, J.F., Plessen, B., Marwan, Bradbury, H.J., Hartland, A., French, A.D., Breitenbach, S.F., 2023. Recurring summer and winter droughts from 4.2-3.97 thousand years ago in north India. Communications Earth & Environment 4, 103.

Griffiths, M.L., Drysdale, R.N., Gagan, M.K., Zhao, J.X., Ayliffe, L.K., Hellstrom, J.C., Hantoro, W.S., Frisia, S., Feng, Y.X., Cartwright, I., Pierre, E.S., 2009. Increasing Australian–Indonesian monsoon rainfall linked to early Holocene sea-level rise. Nat. Geosci. 2, 636–639.

Gong, D.T., Ho, C.H., 2002. The Siberian High and climate changes over middle to high latitude of Asia. Theor. Appl. Climatol. 72, 1–9.

Hartland, A., Fairchild, I.J., Lead, J.R., Baker, A., 2010. Fluorescent properties of organic carbon in cave dripwaters: effects of filtration, temperature and pH. Sci. Total Environ. 408, 5940–5950.

Hellstrom, J.C., 2003. Rapid and accurate U/Th dating using parallel ion-counting multi-collector ICP-MS. J. Anal. Atomic Spectrom. 18, 135–136.

Hellstrom, J.C., 2006. U–Th dating of speleothems with high initial ^{230}Th using stratigraphical constraint. Quat. Geochronol. 1, 289–295.

Hendy, C.H., 1971. The isotopic geochemistry of speleothems – I. The calculation of the effect of different modes of formation on the isotopic composition of speleothems and their applicability as palaeoclimatic indicators. Geochem. Cosmochim. Acta 219, 807–824.

Hille, D., 2004. Encyclopedia of Soils in the Environment. Academic Press.

Hua, Q., McDonald, J., Redwood, D., Drysdale, R., Lee, S., Fallon, S., Hellstrom, J., 2012. Robust chronological reconstruction for young speleothems using radiocarbon. Quat. Geochronol. 14, 67–80.

Isola, I., Zanchetta, G., Drysdale, R.N., Regattieri, E., Bini, M., Bajo, P., Hellstrom, J.C., Baneschi, I., Lionello, P., Woodhead, J., Greig, A., 2019. The 4.2 ka event in the central Mediterranean: new data from a Corchia speleothem (Apuan Alps, central Italy). Clim. Past 22, 135–151.

Knorr, W., Prentice, I.C., House, J.I., Holland, E.A., 2005. Long-term sensitivity of soil carbon turnover to warming. Nature 433, 298–301.

Kostrova, S.S., Meyer, H., Fernandoy, F., Werner, M., Tarasov, P.E., 2020. Moisture origin and stable isotope characteristics of precipitation in southeast Siberia. Hydrol. Process. 34 (1), 51–67.

Kurita, N., Yoshida, N., Inoue, G., Chayanova, E.A., 2004. Modern isotope climatology of Russia: a first assessment. J. Geophys. Res. 109, 03102.

Labban, A.H., Mashat, A.W.S., Awad, A.M., 2021. The variability of the Siberian high ridge over the Middle East. Int. J. Climatol. 41, 104–130.

Lechleitner, F.A., Mason, A.J., Breitenbach, S.F., Vaks, A., Haghipour, N., Henderson, G. M., 2020. Permafrost-related hiatuses in stalagmites: evaluating the potential for reconstruction of carbon cycle dynamics. Quat. Geochronol. 56, 101037.
Lechleitner, F.A., Day, C.C., Kost, O., Wilhelm, M., Haghipour, N., Henderson, G.M., Stoll, H.M., 2021. Stalagmite carbon isotopes suggest deglacial increase in soil respiration in western Europe driven by temperature change. Clim. Past 17, 1903–1918.
Li, T.Y., Baker, J.L., Wang, T., Zhang, J., Wu, Y., Li, H.C., Blyakharchuk, T., Yu, T.L., Shen, C.C., Cheng, H., Kong, X.G., 2021. Early Holocene permafrost retreat in West Siberia amplified by reorganization of westerly wind systems. Communications Earth & Environment 2, 199.
Linge, H., Lauritzen, S.-E., Lundberg, J., Berstad, M., 2001. Stable isotope stratigraphy of Holocene speleothems: examples from a cave system in Rana, northern Norway. Palaeogeogr. Palaeoclimatol. Palaeoecol. 167, 209–224.
Liu, F., Feng, Z., 2012. A dramatic climatic transition at ~4000 cal.yr BP and its cultural responses in Chinese cultural domain. Holocene 22, 1181–1197.
Magny, M., Haas, J.N., 2004. A major widespread climatic change around 5300 cal. yr BP at the time of the Alpine Iceman. J. Quat. Sci. 19, 423–430.
Magny, M., Vanniere, B., Zanchetta, G., Fouache, E., Touchias, G., Petrika, L., Coussot, C., Walter-Simonnet, A.-V., Arnoud, F., 2009. Possible complexity of the climatic event around 4300-3800 cal. BP in the central and western Mediterranean. Holocene 19, 1–11.
Magny, M., Combourieu-Nebout, N., De Beaulieu, J.L., Bout-Roumazeilles, V., Colombaroli, D., Desprat, S., Francke, A., Joannin, S., Ortu, E., Peyron, O., Revel, M., 2013. North–south palaeohydrological contrasts in the central Mediterranean during the Holocene: tentative synthesis and working hypotheses. Clim. Past 9, 2043–2071.
Mariko, S., Nishimura, N., Mo, W., Matsui, Y., Kibe, T., Koizumi, H., 2000. Winter CO_2 flux from soil and snow surface in a cool-temperate deciduous forest. Japan. Ecol. Res. 15, 363–372.
Marino, G., Rohling, E.J., Sangiorgi, F., Hayes, A., Casford, J.L., Lotter, A.F., Kucera, M., Brinkhuis, H., 2009. Early and middle Holocene in the Aegean Sea: interplay between high and low latitude climate variability. Quat. Sci. Rev. 28, 3246–3262.
Martín-Chivelet, J., Muñoz-García, M.B., Cruz, J.A., Ortega, A.I., Turrero, M.J., 2017. Speleothem Architectural Analysis: integrated approach for stalagmite-based paleoclimate research. Sediment. Geol. 353, 28–45.
Mayewski, P.A., Meeker, L.D., Twickler, M.S., Whitlow, S., Yang, Q., Lyons, W.B., Prentice, M., 1997. Major features and forcing of high latitude Northern Hemisphere atmospheric circulation using 110 000-year long glaciochemical series. J. Geophys. Res. 102, 345–366.
McDermott, F., 2004. Palaeo-climate reconstruction from stable isotope variations in speleothems: a review. Quat. Sci. Rev. 23, 901–918.
McGarry, S., Baker, A., 2000. Organic acid fluorescence: applications to speleothem palaeoenvironmental reconstruction. Quat. Sci. Rev. 19, 1087–1101.
Meeker, L.D., Mayewsky, P.A., 2002. A 1400-year high-resolution record of atmospheric circulation over the North Atlantic and Asia. Holocene 12, 257–266.
Mikhailova, A.B., Grenaderova, A.V., Kurina, I.V., Shumilovskikh, L.S., Stojko, T.G., 2021. Holocene vegetation and hydroclimate changes in the Kansk forest steppe, Yenisei River basin, east Siberia. Boreas 4, 948–966.
Mickler, P.J., Stern, L.A., Banner, J.L., 2006. Large kinetic isotope effects in modern speleothems. Geol. Soc. Am. Bull. 118, 65–81.
Morley, D.W., Leng, M.J., Mackay, A.W., Sloane, J.H., 2005. Late glacial and Holocene environmental change in the Lake Baikal region documented by oxygen isotopes from diatom silica. Global Planet. Change 46, 221–233.
Moseley, G.E., Spötl, C., Brandstätter, S., Erhardt, T., Luetscher, M., Edwards, R.L., 2020. NALPS19: sub-orbital-scale climate variability recorded in northern Alpine speleothems during the last glacial period. Clim. Past 16, 29–50.
Mühlinghaus, C., Scholz, D., Mangini, A., 2009. Modelling fractionation of stable isotopes in stalagmites. Geochem. Cosmochim. Acta 73, 7275–7289.
Noronha, A.L., Johnson, K.R., Hu, C., Ruan, J., Southon, J.R., Ferguson, J.E., 2014. Assessing influences on speleothem dead carbon variability over the Holocene: implications for speleothem-based radiocarbon calibration. Earth Planet Sci. Lett. 394, 20–29.
Oster, J.L., Montañe, I.P., Sharp, W.D., Cooper, K.M., 2009. Late Pleistocene California droughts during deglaciation and Arctic warming. Earth Planet Sci. Lett. 288, 434–443.
Panagiotopoulos, F., Shahgedanova, M., Hannachi, A.W., Stephenson, D.B., 2005. Observed trends and teleconnections of the SH: a recently declining center of action. J. Clim. 18, 1411–1422.
Pearson, A.R., Hartland, A., Frisia, S., Fox, B.R., 2020. Formation of calcite in the presence of dissolved organic matter: partitioning, fabrics and fluorescence. Chem. Geol. 539, 119492.
Pérez-Mejías, C., Moreno, A., Sancho, C., Martín-García, R., Spotl, C., Cacho, I., Cheng, H., Edwards, L., 2019. Orbital-to-millennial scale climate variability during marine isotope stages 5 to 3 in northeast iberia. Quat. Sci. Rev. 224, 105946.
Perrette, Y., Poulenard, J., Protière, M., Fanget, B., Lombard, C., Miège, C., Quiers, M., Nafferchoux, E., Pépin-Donat, B., 2015. Determining soil sources by organic matter EPR fingerprints in two modern speleothems. Org. Geochem. 88, 59–68.
Perşoiu, A., Ionita, M., Weiss, H., 2019. Atmospheric blocking induced by the strengthened Siberian High led to drying in west Asia during the 4.2 ka BP event–a hypothesis. Clim. Past 15, 781–793.
Piccini, L., Zanchetta, G., Drysdale, R.N., Hellstrom, J., Isola, I., Fallick, A.E., Leone, G., Doveri, M., Mussi, M., Mantelli, F., Molli, G., Lotti, L., Roncioni, A., Regattieri, E., Meccheri, M., Vaselli, L., 2008. The environmental features of the Monte Corchia cave system (Apuan Alps, central Italy) and their effects on speleothem growth. Int. J. Speleol. 37, 153–172.
Raich, J.W., Schlesinger, W.H., 1992. The global carbon dioxide flux in soil respiration and its relationship with vegetation and climate. Tellus 44, 81–99.
Regattieri, E., Forti, L., Drysdale, R.N., Mannella, G., Hellstrom, J.C., Conati Barbaro, C., Zerboni, A., 2023. Neolithic hydroclimatic change and water resources exploitation in the Fertile Crescent. Sci. Rep. 13, 45.
Regattieri, E., Isola, I., Zanchetta, G., Tognarelli, A., Hellstrom, J.C., Drysdale, R.N., Boschi, C., Milevski, I., Temovski, M., 2019. Middle-holocene climate variability from a stalagmite from alilica cave (southern Balkans). Alpine and Mediterranean Quaternary 32.
Regattieri, E., Zanchetta, G., Drysdale, R.N., Isola, I., Hellstrom, J.C., Dallai, L., 2014. Lateglacial to Holocene trace element record (Ba, Mg, Sr) from Corchia cave (apuan Alps, central Italy): paleoenvironmental implications. J. Quat. Sci. 29, 381–392.
Riaz, S.M.F., Iqbal, M.J., Baig, M.J., 2018. Influence of Siberian high on temperature variability over northern areas of South Asia. Meteorol. Atmos. Phys. 130, 441–457.
Rohling, E.J., Marino, G., Grant, K.M., Mayewski, P.A., Weninger, B.A., 2019. Model for archaeologically relevant Holocene climate impacts in the Aegean-Levantine region (easternmost Mediterranean). Quat. Sci. Rev. 208, 38–53.
Rohling, E.J., Mayewski, P.A., Abu-Zied, R.H., Casford, J.S.L., Hayes, A., 2002. Holocene atmosphere-ocean interactions: records from Greenland and the Aegean Sea. Clim. Dynam. 18, 587–593.
Roland, T.P., Caseldine, C.J., Charman, D.J., Turney, C.S.M., Amesbury, M.J., 2014. Was there "4.2ka event" in Great Britain and Ireland? Evidence from peatland record. Quat. Sci. Rev. 83, 11–27.
Rudaya, N., Tarasov, P., Dorofeyuk, N., Solovieva, N., Kalugin, I., Andreev, A., Dayin, A., Diekmann, B., Riedel, F., Tserendash, N., Wagner, M., 2009. Holocene environments and climate in the Mongolian Altai reconstructed from the Hoton-Nur pollen and diatom records: a step towards better understanding climate dynamics in Central Asia. Quat. Sci. Rev. 28, 540–554.
Rudzka, D., McDermott, F., Baldini, L.M., Fleitmann, D., Moreno, A., Stoll, H., 2011. The coupled δ^{13}C-radiocarbon systematics of three Late Glacial/early Holocene speleothems: insights into soil and cave processes at climatic transitions. Geochem. Cosmochim. Acta 75, 4321–4339.
Shapov, Y.Y., Ford, D.C., Schwarcz, H.P., 1994. Luminescent microbanding in speleothems: high-resolution chronology and paleoclimate. Geology 22, 407–410.
Staubwasser, M., Weiss, H., 2004. Holocene climate and cultural evolution in the late prehistoric-early West Asia. Quat. Res. 66, 372–387.
Solomon, D.K., Cerling, T.E., 1987. The annual carbon dioxide cycle in a montane soil: Observations, modeling, and implications for weathering. Water Resour. Res. 23 (12), 2257–2265.
Spötl, C., Mangini, A., 2007. Speleothems and paleoglaciers. Earth Planet Sci. Lett. 254, 323–331.
Stoll, H.M., Day, C., Lechleitner, F., Kost, O., Endres, L., Sliwinski, J., Pérez-Mejías, C., Cheng, H., Scholz, D., 2022. Distinguishing the vegetation and soil component of δ^{13}C variation in speleothem records from degassing and prior calcite precipitation effects. Clim. Past.
Swift, M.J., Heal, O.W., Anderson, J.M., 1979. Decomposition in Terrestrial Ecosystems. Blackwell Scientific Publications, Oxford, p. 372.
Sundqvist, H.S., Holmgren, K., Moberg, A., Spötl, C., Mangini, A., 2010. Stable oxygen isotopes in a stalagmite from Jämtland, NW Sweden, record large temperature variations over the last 4000 years. Boreas 39, 77–86.
Tremaine, D.M., Froelich, P.N., Wang, Y., 2011. Speleothem calcite farmed in situ: modern calibration of δ^{18}O and δ^{13}C paleoclimate proxies in a continuously-monitored natural cave system. Geochem. Cosmochim. Acta 75, 4929–4950.
Tubi, A., Dayan, U., 2013. The Siberian High: teleconnections, extremes and association with Iceland Low. Int. J. Climatol. 33, 1357–1366.
Turetsky, M.R., Abbott, B.W., Jones, M.C., Anthony, K.W., Olefeldt, D., Schuur, E.A., Grosse, G., Kuhry, P., Hugelius, G., Koven, C., Lawrence, D.M., 2020. Carbon release through abrupt permafrost thaw. Nat. Geosci. 13, 138–143.
Vaks, A., Gutareva, O.S., Breitenbach, S.F.M., Avirmed, E., Mason, A.J., Thomas, A.L., Osinzev, A.V., Kononov, A.M., Henderson, G.M., 2013. Speleothems reveal 500,000-year history of Siberian permafrost. Science 34, 183–186.
Vaks, A., Mason, A.J., Breitenbach, S.F., Kononov, A.M., Osinzev, A.V., Rosensaft, M., Borshevsky, A., Gutareva, O.S., Henderson, G.M., 2020. Palaeoclimate evidence of vulnerable permafrost during times of low sea ice. Nature 577, 221–225.
Wang, Y.J., Cheng, H., Edwards, R.L., An, Z.S., Wu, J.Y., Shen, C.C., Dorale, J.A., 2001. A high resolution absolute-dated late Pleistocene monsoon record from Hulu Cave, China. Science 294, 2345–2348.
Wang, T., Li, T.Y., Zhang, J., Wu, Y., Chen, C.J., Huang, R., Li, J.Y., Xiao, S.Y., Artemevna Blyakharchuk, T., 2020. A climatological interpretation of precipitation δ^{18}O across Siberia and Central Asia. Water 12, 2132.
Weiss, H., Courty, M.A., Wetterstrom, W., Guichard, F., Senior, L., Meadow, R., Curnow, A., 1993. The genesis and collapse of third millennium North Mesopotamian civilization. Science 261, 995–1004.
Wilcox, P.S., Dorale, J.A., Baichtal, J.F., Spotl, C., Fowell, S.J., Edwards, R.L., Kovarik, J. L., 2019. Millennial-scale glacial climate variability in Southeastern Alaska follows Dansgaard-Oeschger cyclicity. Sci. Rep. 9, 7880.
Winston, G.C., Sundquist, E.T., Stephens, B.B., Trumbore, S.E., 1997. Winter CO_2 fluxes in a boreal forest. J. Geophys. Res. 102, 795.
Wirtz, K.W., Lohmann, G., Bernhardt, K., Lemmen, C., 2010. Mid-Holocene regional reorganization of climate variability: analyses of proxy data in the frequency domain. Paleogeography, Palaeoclimatology, Palaeocology 298, 189–200.
Wu, B., Wang, J., 2002. Winter arctic oscillation, SH and East Asian winter monsoon. Geophys. Res. Lett. 29, 1897.
Yancheva, G., Nowaczyk, N.R., Mingram, J., Dulski, P., Schettler, G., Negendank, J.F., Liu, J., Sigman, D.M., Peterson, L.C., Haug, G.H., 2007. Influence of the intertropical convergence zone on the East Asian monsoon. Nature 445, 74–77.

Yuan, D., Cheng, H., Edwards, R.L., Dykoski, C.A., Kelly, M.J., Zhang, M., Qing, J., Lin, Y., Wang, Y.J., Wu, J.Y., Dorale, J.A., An, Z.S., Cai, Y.J., 2004. Timing, duration, and transitions of the last interglacial asian monsoon. Science 304, 575–578.

Zanchetta, G., Bar-Matthews, M., Drysdale, R.N., Lionello, P., Ayalon, A., Hellstrom, J.C., Isola, I., Regattieri, E., 2014. Coeval dry events in the central and eastern Mediterranean basin at 5.2 and 5.6 ka recorded in Corchia (Italy) and Soreq caves (Israel) speleothems. Global Planet. Change 122, 130–139.

Zanchetta, G., Regattieri, E., Isola, I., Drysdale, R.N., Baneschi, I., Hellstrom, J.C., 2016. The so-called "4.2 event" in the central Mediterranean and its climatic teleconnections. Alpine and Mediterranean Quaternary 29, 5–17.

Zhang, M., Bu, Z., Jiang, M., Wang, S., Liu, S., Jin, Q., Shi, P., 2019. Mid-late Holocene maar lake-mire transition in northeast China triggered by hydroclimatic variability. Quat. Sci. Rev. 220, 215–229.